

## Study on adsorption of cationic dye on novel *kappa*-carrageenan/poly(vinyl alcohol)/montmorillonite nanocomposite hydrogels

Hossein Hosseinzadeh · Shiva Zoroufi ·  
Gholam Reza Mahdavinia

Received: 14 July 2014 / Revised: 17 January 2015 / Accepted: 19 February 2015 /  
Published online: 28 February 2015  
© Springer-Verlag Berlin Heidelberg 2015

**Abstract** In this study, novel *kappa*-carrageenan/poly(vinyl alcohol) nanocomposite hydrogels were developed by incorporating sodium montmorillonite nanoclay. The mixture of polymers and montmorillonite was crosslinked with freezing–thawing technique and subsequent with  $K^+$  ions. The structure of nanocomposite hydrogels was characterized with the FTIR, SEM, XRD, and TEM techniques. By introducing montmorillonite nanoclay, the swelling capacity of nanocomposites was decreased from 1200 to 320 % due to the crosslinking role of montmorillonite nanoclay. The adsorption of cationic crystal violet dye on nanocomposite hydrogels was studied via batch adsorption system on the subject of contact time, nanoclay content, pH of dye solution, temperature, and ion strength of dye solution. Compared with clay-free hydrogel, the nanocomposites indicated a relatively improved adsorption capacity at the same batch system. The variation in the pH of initial dye solution had no significant effect on dye adsorption capacity of hydrogels. Study on salinity of dye solutions showed that while the NaCl salt had less effect on adsorption capacity of hydrogels, in the presence of  $CaCl_2$  and  $AlCl_3$  salts, the adsorption capacity of nanocomposites was significantly decreased. The adsorption kinetics of crystal violet on hydrogels was well described by the pseudo-second-order model. Also, the equilibrium dye adsorption data were analyzed with non-linear Langmuir and Freundlich models and the equilibrium process was followed well the Langmuir model. According to the Langmuir model, the maximum adsorption capacity of nanocomposites was obtained  $151 \text{ mg g}^{-1}$ . Thermodynamic parameters confirmed the spontaneity of the adsorption process. Therefore, the

---

H. Hosseinzadeh (✉) · S. Zoroufi  
Chemistry Department, Payame Noor University, 19395-4697 Tehran, Iran  
e-mail: h\_hosseinzadeh@pnu.ac.ir

G. R. Mahdavinia  
Chemistry Department, Faculty of Science, University of Maragheh,  
P.O. Box 55181-83111, Maragheh, Iran

synthesized hydrogel nanocomposites could be employed as a low-cost adsorbent in the removal of dyes from aqueous solution.

**Keywords** *Kappa*-carrageenan · Hydrogel · Nanocomposite · Poly(vinyl alcohol) · Montmorillonite · Adsorption · Crystal violet

## Introduction

The blending of polymers is an efficient and simple route to improve the cost-effectiveness of commercial products [1]. Recently, the polymer–inorganic nanocomposites based on synthetic/natural polymers by incorporation of inorganic layered silicates have attracted both academia and industry because of their unique properties [2–4]. Alternatively, synthesizing interpenetrating polymer network (IPN) is a well-known way to force the compatibility of immiscible polymers [5]. IPN is an intimate combination of two polymers both in the same network, which is obtained when at least one polymer is synthesized and/or crosslinked independently in the immediate vicinity of the other [6]. A semi-interpenetrating networks (semi-IPNs) which consist of both linear and crosslinked polymer have been used to improve the properties of polymer blends and composites. Carrageenans are linear sulfate polysaccharides that are obtained by extraction from certain edible species of red seaweeds [7]. Because of their exceptional properties, carrageenans are widely used as ingredients in a variety of applications. They have several major characteristics that make them very useful in just about any food and non-food applications. Since carrageenan is a highly negatively charged macromolecule, it can be able to interact with any species carrying a positive charge. Many reports are published in this regard such as interaction of carrageenan with univalent and divalent cations [8], gelatin [9], and chitosan [10].

Since *kappa*-carrageenan contains high contents of sulfate and hydroxyl functional groups, it may potentially be miscible with poly(vinyl alcohol) (PVA) due to the formation of hydrogen bonds. PVA has been extensively used in many biomaterial applications due to its unique properties such as: easy preparation, good biodegradability, excellent chemical resistance, good mechanical properties, processability and good chemical resistance [11]. In addition, because of the strong hydrophilic and hydrogen bonding character of PVA, it can form new materials which can be applied in medicine and pharmaceutical industry [11]. However, low gel strength, poor mechanical reliability, and low fracture toughness have limited its application. The freezing–thawing method is regarded the best and the preferred physically crosslinking method for overcoming these limitations without using any traditional toxic chemical crosslinking agent [12]. It is generally accepted that PVA chains can undergo crosslinking via a freeze–thaw process and the degree of crosslinking increases with the number of cycles [13]. PVA networks prepared by this method show many useful properties like high mechanical strength, rubberlike elasticity, stability at room temperature, ability to retain their original shape, high water content, biocompatibility, and lack of toxicity [14].

Hydrogels are three-dimensional polymeric networks capable of holding large quantities of water in its structure [15]. Polymer hydrogels have gained great attention in wide variety of biomedical applications such as wound dressings [16], contact lenses [17], artificial organs [18], tissue engineering [19] and drug delivery systems [20, 21] due to their unique swelling behaviors. However, poor mechanical properties of hydrogels are serious impediments that must be resolved for their commercial applications [22]. To date, most conventional hydrogels are crosslinked by organic compounds. However, an inhomogeneous randomly crosslinked network often makes the hydrogel weak and fragile, which limits its application seriously [23].

In recent studies, polymer–clay nanocomposite hydrogels have been extensively studied to improve the mechanical strength and swelling properties [24, 25]. In the initial phase of the development of nanocomposite hydrogels, various clay minerals were widely added to polymer hydrogels matrix to improve their weak mechanical stability [26–28]. Among them, montmorillonite and attapulgite were extensively used as reinforcing fillers in the preparation of nanocomposite hydrogels [29, 30]. The incorporation of inorganic layered silicates into pure polymeric networks with uniform dispersion not only can improve the water-absorbing properties and the gel strength of the resultant absorbing materials, but also can reduce the final production cost [31].

Removal of dyes is nowadays regarded as an important practice in textile wastewater treatment. Numerous methods have been used to decolorize dye from aqueous solutions. However, most of these methods are generally expensive. As a consequence, there has been considerable effort directed toward development of low-cost adsorbents for dye removal [32]. Because of low cost, abundance, and high sorption capacities, natural-based hydrogel nanocomposites are interesting materials for use as adsorbents. Hence, many researchers recently have studied the feasibility of using natural polymers for the removal of various dyes [33–37]. Carrageenans are relatively new polysaccharides in the synthesis of natural-based dye adsorbent polymers. In this work, the main idea for synthesis of carrageenan-based adsorbent is originated from the presence of hydrophilic sulfate groups in its backbones with high ionization tendency which increases the charge density in final product. Moreover, the presence of the natural parts guarantees biodegradability of the adsorbing materials.

Although different hydrogels were developed by incorporation of carrageenan and poly(vinyl alcohol) [38–42], study on preparation, characterization and adsorption properties of carrageenan–PVA hydrogels for removal of dyes has not yet been studied extensively. Therefore, following continuous research on synthesis of hydrogel nanocomposites based on carrageenan [43–46], we attempted to prepare carrageenan–PVA–montmorillonite nanocomposites. To nutshell, we studied the structure of nanocomposite hydrogels and investigated the swelling of nanocomposites. Crystal violet as a model dye was selected to study the adsorption behavior of synthesized hydrogels.

## Experimental

### Materials

The polysaccharide, *kappa*-carrageenan ( $\kappa$ C, from Condinson Co., Denmark), sodium montmorillonite (NaMMT, from Southern Clay), poly(vinyl alcohol) (PVA, MW 89,000–98,000; degree of hydrolysis 99 %, from Aldrich Chemicals), and crystal violet (CV, from Difko Chemical Company, UK) were used without further purification. The molecular structure and identification information of crystal violet dye are depicted in Table 1.

### Preparation of hydrogel nanocomposites

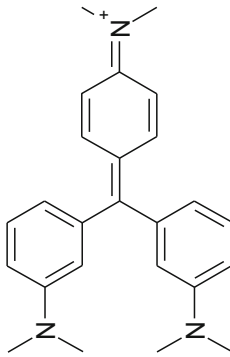
A general procedure for the synthesis of the  $\kappa$ C-based hydrogel nanocomposites was conducted as follows. 1.0 g of PVA was added in 50 mL of doubly distilled water at 70 °C. After complete dissolution of PVA, 1.0 g of  $\kappa$ C was added to the solution and the mixture stirred until complete dissolution of  $\kappa$ C. Then, an appropriate weight of the NaMMT nanoclay [0 g, Mont (zero); 0.1 g, Mont (0.1); 0.2 g, Mont (0.2); 0.4 g, Mont (0.4); and 0.6 g, Mont (0.6)] was added to the polymers solution and allowed to stir at 70 °C for 20 min. The resulted solution was then sonicated for 20 min at 80 °C to obtain a homogeneous solution. The operating frequency used in sonication was 70 kHz. At first, the sonicated solution containing PVA,  $\kappa$ C, and NaMMT was cooled to ambient temperature and the products were kept frozen at –20 °C for overnight. The frozen hydrogels were thawed at ambient temperature for 5 h. The process involved freezing–thawing was repeated 4 times. After freezing–thawing steps, the hydrogels were immersed into 0.5 M of KCl solution for 60 min to provide mechanically acceptable hydrogels for further experiments. The crosslinked nanocomposite hydrogels were immersed into excess distilled water for purification for overnight. Finally, the hydrogels were cut into discs with 0.5 mm radius and 0.4 mm thickness and dried at room temperature for constant weight.

### Swelling measurements

Dried discs were used to determine the water absorbency of hydrogels. The equilibrium swelling (ES) capacity was determined by immersing the nanocomposites (~0.1 g) in 50 mL of distilled water and allowed to swell at room temperature for certain times (10–250 min). Then, they were removed from aqueous solutions and blotted with filter paper to remove surface water, weighed and the percentage of ES was calculated twice using Eq. (1):

$$\text{ES (\%)} = \frac{\text{Weight of swollen hydrogel} - \text{Weight of dried hydrogel}}{\text{Weight of dried hydrogel}} \times 100 \quad (1)$$

**Table 1** The chemical structure and some properties of CV

IUPAC name	Chemical structure	Molar mass (g mol <sup>-1</sup> )	Color index number	$\lambda_{\text{max}}$ (nm)
Tris(4-(dimethylamino)phenyl)methylium		407.98	42,555	590

## Adsorption studies

Adsorption of CV dye on nanocomposites was carried out by immersing the  $\sim 0.05$  g of samples into dye solution (50 mL,  $25 \text{ mg L}^{-1}$  of CV). All adsorption experiments were examined through a batch method on a shaker with a constant speed at 120 rpm and at ambient temperature ( $25 \text{ }^\circ\text{C}$ ). To study the adsorption kinetics, at specified time intervals, the amount of adsorbed CV was evaluated using a UV spectrometer at  $\lambda_{\text{max}} = 595 \text{ nm}$ . The solutions were centrifuged (at 3000 rpm for 10 min) before measurements. The content of adsorbed dye was calculated twice using Eq. (2):

$$q_t = \frac{(C_0 - C_t) \times V}{W} \quad (2)$$

where  $C_0$  is the initial CV concentration ( $\text{mg L}^{-1}$ );  $C_t$  is the remaining dye concentration in the solution at time  $t$ ;  $V$  is the volume of dye solution used (L); and  $W$  (g) is the weight of nanocomposite. Adsorption isotherm was carried out by immersing of 0.05 g of nanocomposites into 50 mL of dye solutions with 25, 50, 100, 150, and 200  $\text{mg L}^{-1}$  of CV at  $25 \text{ }^\circ\text{C}$  for 24 h. The equilibrium adsorption capacity of nanocomposites,  $q_e$  ( $\text{mg g}^{-1}$ ), was determined using Eq. (2). At this Equation, the  $C_t$  and the  $q_t$  will be replaced with equilibrium concentration of dye in the solution ( $C_e$ ) and equilibrium adsorption capacity ( $q_e$ ), respectively. To investigate the effect of pH on adsorption, the pH of initial dye solution was adjusted by the addition of 0.1 M HCl or 0.1 M NaOH solutions.

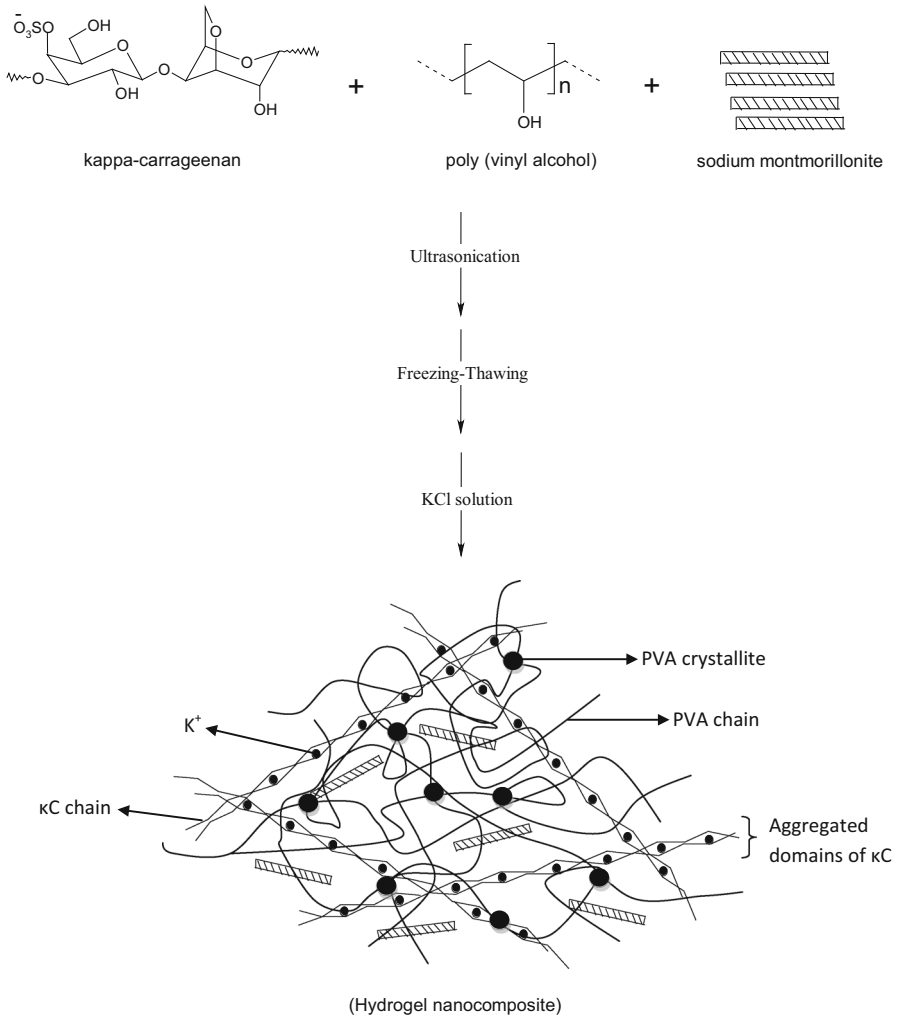
## Instrumental analysis

Fourier transform infrared (FTIR) spectroscopy absorption spectra of samples were taken in KBr pellets, using an FTIR spectrophotometer (Bruker, Germany) at room temperature. The surface morphology of the hydrogel was examined using scanning electron microscopy (SEM). Samples for SEM were prepared by specific time dried in room condition ( $25 \text{ }^\circ\text{C}$ ). Dried powder sample was coated with a thin layer of palladium gold alloy and imaged in a SEM instrument (Vega-Tescan, Czech Republic). Transmission electron microscopy (TEM) micrographs were recorded with a Philips CM10 (UK) operating at 60 kV tension. The X-ray diffraction patterns of samples were also recorded using a Siemens D-500 X-ray diffractometer with wavelength  $\lambda = 1.54 \text{ \AA}$  ( $\text{Cu-K}\alpha$ ), at a tube voltage of 35 kV, and tube current of 30 mA.

## Results and discussion

### Mechanism of preparation of hydrogel nanocomposite

Scheme 1 displays a simple method for preparation of a novel semi-interpenetrating polymer network (semi-IPN) hydrogel nanocomposite composed of a mixture of *kappa*-carrageenan ( $\kappa\text{C}$ ) and poly(vinyl alcohol) by incorporation of sodium



**Scheme 1** Proposed mechanistic pathway for synthesis of κC-PVA/NaMMT semi-IPN hydrogel nanocomposite

montmorillonite (NaMMT). To obtain hydrogel nanocomposites, the crosslinking of the mixture was done in two stages. First, the freezing–thawing method was applied to crosslink the PVA component [47]. In fact, the PVA molecular chains were associated fully through hydrogen bonds during the freezing/thawing process. Moreover, as the PVA chains come into close contact with each other, crystallite formation occurs [48]. So, the repeated freezing–thawing cycles cause to a non-degradable three-dimensional structure in physical PVA networks, leading to the formation of the compact product with high mechanical strength. Several researchers have shown evidence of hydrogen bonding and crystallite formation [49–52]. After freezing–thawing for 4 times, the hydrogels were transferred into

KCl solution for crosslinking of the  $\kappa$ C component. The anionic sulfate groups on  $\kappa$ C backbones can be interacted electrostatically with  $K^+$  cations and led to crosslink of  $\kappa$ C component. Several papers have reported the interaction of *kappa*-carrageenans with cations such as  $K^+$ ,  $Na^+$  and  $Ca^{2+}$  to form ionically crosslinked helical molecules [53–55]. Carrageenans are aggregated with various cations and degree of aggregation is strongly dependent on the type and concentration of salt added to the carrageenan solution. In general, the mechanism of crosslinking of  $\kappa$ C chains by  $K^+$  ions was previously investigated by a Domain model [53] using a double helix formation. According to this model, direct intermolecular association through double helices is confined to the formation of small independent domains involving a limited number of chains, and more long-range crosslinking is by association between helices in different domains. On the basis of this accepted model, the mechanism of gelation is outlined schematically in Scheme 1. It may be noted that NaMMT can act as co-crosslinker of hydrophilic polymers in solution due to the formation of hydrogen bonding between silanol groups ( $-Si-OH$ ) on the layer surface of montmorillonite and hydrophilic functional groups on polymer backbones [56].

## Characterization

After introducing montmorillonite to the polymer structure, the resulting nanocomposite hydrogels have different changes such as the structural characteristics that are discussed below.

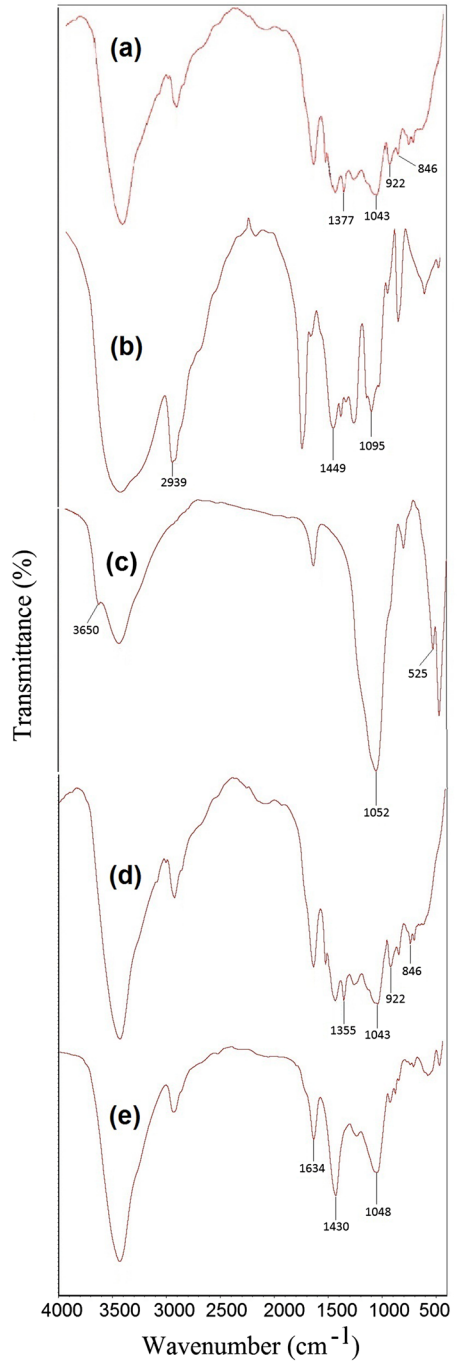
### FTIR analysis

Fourier transform infrared (FTIR) spectroscopy is an analytical technique used to identify especially organic materials. This technique measures the absorption of infrared radiation by the sample versus wavelength. The infrared absorption bands identify molecular components and structures. In fact, the wavelengths that are absorbed by the sample are characteristic of its molecular structure. To investigate the information on the structure of the  $\kappa$ C–PVA/MMT nanocomposites, infrared spectroscopy was firstly used.

Figure 1 shows the FTIR spectra of raw materials (i.e.,  $\kappa$ C, PVA, NaMMT), clay-free hydrogel [Mont (zero)], and the hydrogel nanocomposite [Mont (0.2)]. In the spectrum of  $\kappa$ C (Fig. 1a), the bands observed at 846, 922, 1043 and  $1377\text{ cm}^{-1}$  can be attributed to the D-galactose-4-sulfate, 3,6-anhydro-D-galactose, glycosidic linkage and ester sulfate stretching of  $\kappa$ C, respectively. The broad band at  $3200\text{--}3400\text{ cm}^{-1}$  is due to stretching of  $-OH$  groups of substrate. The FTIR spectrum of pure PVA (Fig. 1b) included the C–O stretching band at around  $1095\text{ cm}^{-1}$ , C–C stretching band at around  $1449\text{ cm}^{-1}$ , C–H stretching band at around  $2939\text{ cm}^{-1}$ , broad O–H stretching band at around  $3200\text{--}3600\text{ cm}^{-1}$ . For the pristine NaMMT (Fig. 1c), the characteristic bands at around 525 and  $1052\text{ cm}^{-1}$  were assigned to the Si–O stretching bands in the structure of the nanoclay. And the small band at around  $3650\text{ cm}^{-1}$  was attributed to the O–H stretching band of the nanoclay.



**Fig. 1** FTIR spectra of  $\kappa$ C (a), PVA (b), NaMMT (c), pure hydrogel without NaMMT (d), and the hydrogel nanocomposite containing 0.2 g of NaMMT (e)



The hydrogel nanocomposite product comprises crosslinked  $\kappa$ C and PVA backbones incorporated with NaMMT. Compared to clay-free hydrogel (Fig. 1d), intense of some of the sulfate stretching of  $\kappa$ C in the hydrogel nanocomposite (Fig. 1e) was diminished that established the hydrogen bonding formation and crosslinking between these groups and Si–OH on the layer surface of NaMMT nanoclay. Also, for the  $\kappa$ C–PVA/MMT nanocomposite samples, the C–O stretching band of PVA and the Si–O stretching band of clay were overlapped slightly to become a broader band at around  $1048\text{ cm}^{-1}$ . This band indicated the presence of Si–O group due to the clay layer in the nanocomposite samples. Besides, the O–H stretching bands of the MMT clay (at around  $3650\text{ cm}^{-1}$ ) were shifted to lower wave number and towards the O–H stretching bands of the PVA (at around  $3200\text{--}3450\text{ cm}^{-1}$ ) and they combined together to become broader hydroxyl stretching band. In brief, FTIR indicated that introducing NaMMT into  $\kappa$ C and PVA chains caused some interactions between the silanol and functional groups on polymers.

### SEM and TEM analysis

Scanning electron microscopy (SEM) is a method for high-resolution imaging of surfaces. The SEM uses a focused beam of high-energy electrons to generate a variety of signals at the surface of solid specimens. The electrons interact with atoms in the sample, producing various signals that can be detected and that contain information about the sample's surface topography and composition. Therefore, the SEM images were used to study the morphology of hydrogels. Figure 2 shows the SEM images of the fracture surface of the clay-free hydrogel [Mont (zero), Fig. 2a] and the hydrogel nanocomposites [Mont (0.2) and Mont (0.4), Fig. 2b, c]. As can be seen, the clay-free hydrogel contained a smooth and non-aggregated surface. The surface morphology of nanocomposite hydrogels was not changed remarkably and obtained relatively similar to clay-free hydrogel. These results indicate the well dispersing of clay in nanocomposite matrix.

A transmission electron microscope (TEM) utilizes energetic electrons to provide morphologic, compositional and crystallographic information on samples with very

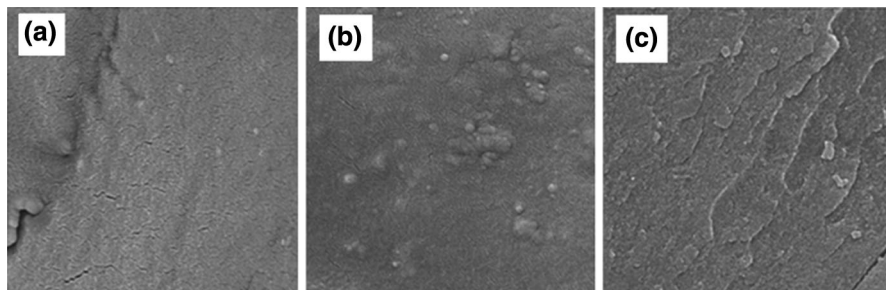


**Fig. 2** SEM images of the fracture surface of the free NaMMT hydrogel **a** and the hydrogel nanocomposites containing 0.2 g **b** and 0.4 g **c** of NaMMT

high spatial resolution. At a maximum potential magnification of 1 nm, TEMs are the most powerful microscopes. TEMs produce high-resolution, two-dimensional black and white images from the interaction that takes place between prepared samples and a high-energy electron beam transmitted through a very thin sample in the vacuum chamber. In the case of nanocomposites, TEM provides very useful information such as the particle size and polydispersity profile of nanoclay. Also, the TEM can be used to study the type of clay dispersion in the polymer composites. Thus, the TEM micrographs of Mont (0.2) and Mont (0.4) were studied and the results shown in Fig. 3a, b. Exfoliated clay layers can be seen in micrograph of Mont (0.2). In fact, when the clay content is low, aggregated sections were not found in nanocomposite matrix. In contrast, not only exfoliated and intercalated clay layers in Mont (0.4) with high content of clay are observed, but also the aggregated sections are appeared.

### *XRD analysis*

X-Ray diffraction (XRD) is a laboratory-based technique commonly used for identifying the atomic and molecular structure of crystalline materials and analysis of unit cell dimensions. In this method, the crystalline atoms cause a beam of incident X-rays to diffract into many specific directions. By measuring the angles and intensities of these diffracted beams, a three-dimensional picture of the density of electrons within the crystal was obtained. XRD is the principal method that has been also used to examine the extent of intercalation and exfoliation. The peak position and the interlayer spacing are two parts of the information provided by XRD measurements. In Fig. 4, XRD patterns of the nanocomposites Mont (0.2) and Mont (0.4) were compared with the pristine NaMMT. According to XRD data, it can be observed that the natural NaMMT shows a strong characteristic peak at  $2\theta = 8.5^\circ$  with a basal spacing of 18 Å (Fig. 4a). However, the absence of this basal peak in nanocomposite Mont (0.2) suggests a high dispersion of clay platelets (exfoliation) in the nanocomposite material (Fig. 4b). The broad and short characteristic peaks of NaMMT with a shifting to low angle in the nanocomposite Mont (0.4) indicated that the platelets of nanoclay have been exfoliated and are thoroughly dispersed in the polymer matrix at nanoscale after crosslinking and

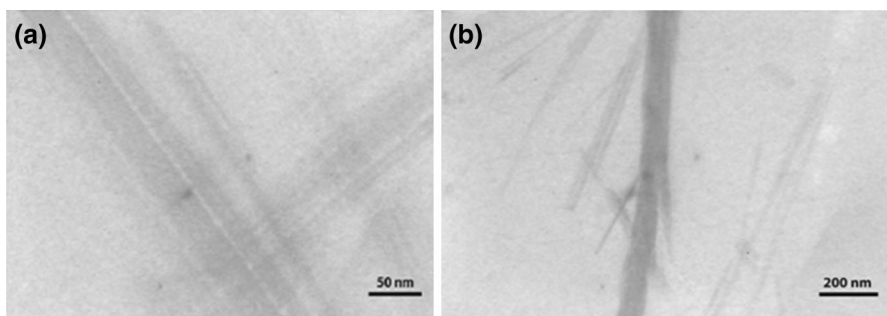


**Fig. 3** TEM images of the hydrogel nanocomposites containing 0.2 g **a** and 0.4 g **b** of NaMMT

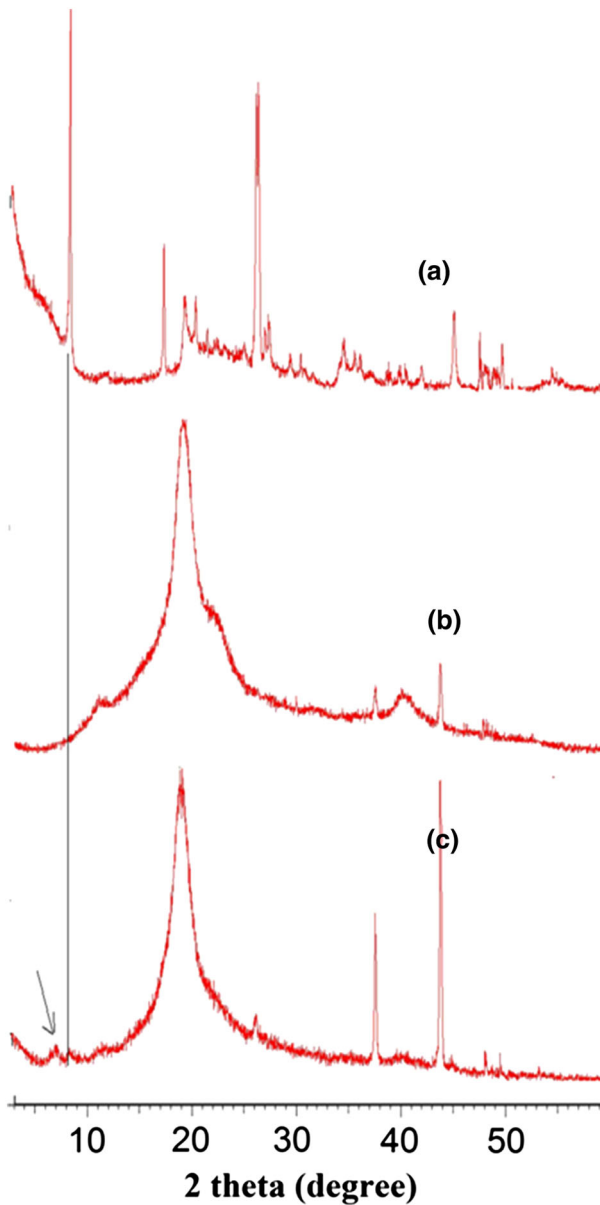


**Fig. 4** XRD patterns of pure NaMMT (a) and the hydrogel nanocomposites containing (b) 0.2 g and (c) 0.4 g of NaMMT

forming a nanocomposite structure (Fig. 4c). Also, in comparison with natural NaMMT, the 001 peak of pristine clay was shifted towards lower angle  $2\theta = 7.0^\circ$  with low intensity, corresponding to a basal spacing of 23 Å. This indicated that by increasing the clay content, in addition to the exfoliation, the expansion of the

interlayer space had occurred because of the intercalation of the polymer molecules. The XRD results confirmed the TEM micrographs of nanocomposites.

### Swelling study

In general, the swelling capacity of hydrogels is strongly influenced by their chemical composition. To understand the effect of NaMMT on the swelling behavior of the hydrogels, the swelling capacity was investigated by varying the nanoclay content from 0.1 up to 0.6 g (Fig. 5). It was clearly observed that the ultimate swelling capacity decreased as the NaMMT amount increased. This observation can be described by the interactions between the NaMMT layers and polymeric chains through formation of hydrogen bonding [56]. This interaction can lead to increase in the crosslinking points and therefore results in decreased swelling capacity [3]. Although with increasing NaMMT content the surface area of the resulted nanocomposites will be increased, but due to the crosslinking role of nanoclays the swelling capacity will be decreased. Meanwhile, the products obtained without applying repeated freezing–thawing cycles do not possess good dimensional stability, so that the swollen gel strength is not sufficient to be referred as a real crosslinked polymer network.

### Dye adsorption study

#### *Effect of pH on dye adsorption*

The pH of the initial dye solution is an important factor in adsorption process. This behavior arises from the nature of the active centers on the adsorbents [57]. To investigate the adsorption of CV dye on adsorbents, the pH of the initial dye

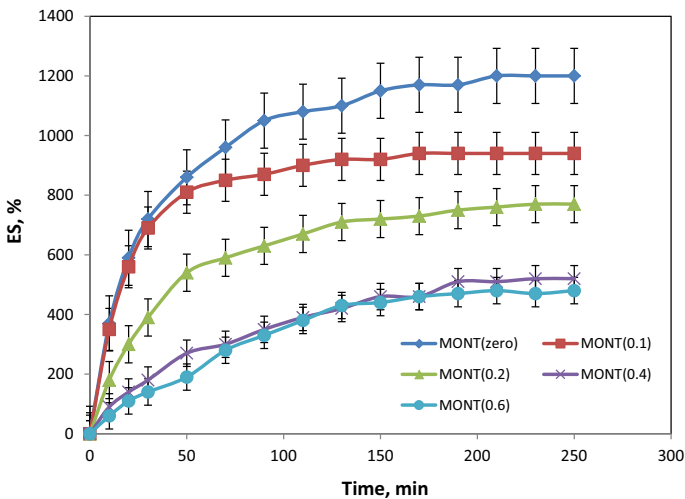


**Fig. 5** The swelling behavior of the pure hydrogel and the hydrogel nanocomposites with various content of NaMMT

solution was changed between 2 and 10 and the results are shown in Fig. 6. During adsorption, the existence of anionic sulfate groups is necessary for the interaction of hydrogel nanocomposite with positively charged CV molecules, as is simply shown in Scheme 2. Compared to hydrogels carrying carboxylate pendants, the adsorption capacity of  $\kappa$ C-based hydrogels for CV was not significantly changed in the pH range of 2–10. This behavior is originated from the  $pK_a$  of anionic sulfate groups on  $\kappa$ C. According to literatures, the  $pK_a$  of these anionic sulfates is around 2 and its ionization occurs above this value [58, 59]. This behavior of the corresponding hydrogels was similar to our previous work discussing about the adsorption of CV dye on nanocomposite hydrogels composed of  $\kappa$ C and alginate biopolymers [46]. At pH 2, a reduction in dye affinity for hydrogels was seen and may be attributed to the screening effect of the counter ions ( $H^+$ ) that restricts the approaching of cationic dye on sulfate groups. In fact, in the overall pH range, these sulfate groups are in the dissociated form. Lower adsorption of CV at acidic pHs is due to the presence of excess  $H^+$  ions competing with the cation groups on the dye for adsorption sites.

#### *Effect of nanoclay content and contact time on dye adsorption*

The effect of both nanoclay content and contact time on the adsorption of CV on hydrogel nanocomposite is shown in Fig. 7. As shown, the adsorption capacity of the nanocomposites increased approximately with an increase in the content of NaMMT. The increase in CV adsorption could be due to the negative surface of the clay. The higher the content of NaMMT in the nanocomposite with a constant weight ratio of  $\kappa$ C and PVA, the higher the concentration of negative charges results in the hydrogel nanocomposites. In fact, nanoclays are already reported as good adsorbents for various adsorbates due to their large specific surface area and high negatively charge density [60]. In a previous work, we reported magnetic adsorbents by incorporating  $\kappa$ C and PVA. When the magnetite nanoparticles incorporated in

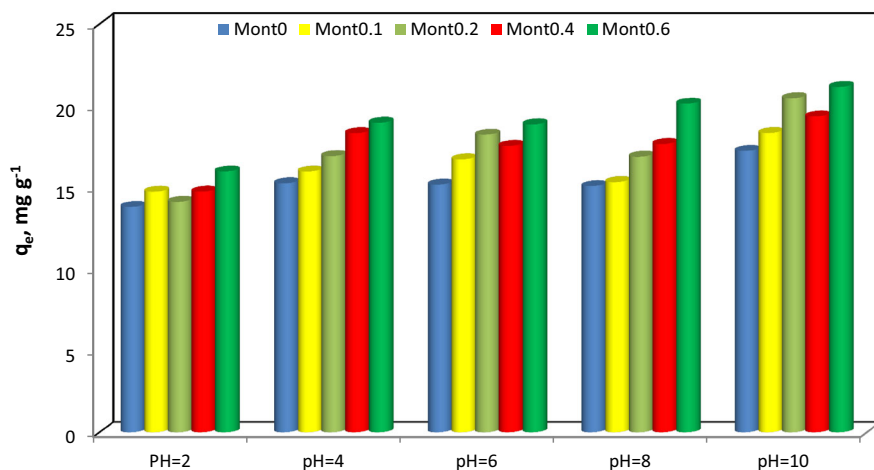


**Fig. 6** Effect of pH of initial dye solution on CV adsorption

**Scheme 2** Electrostatic interactions between negative and positive functional groups of the nanocomposite and dye molecules

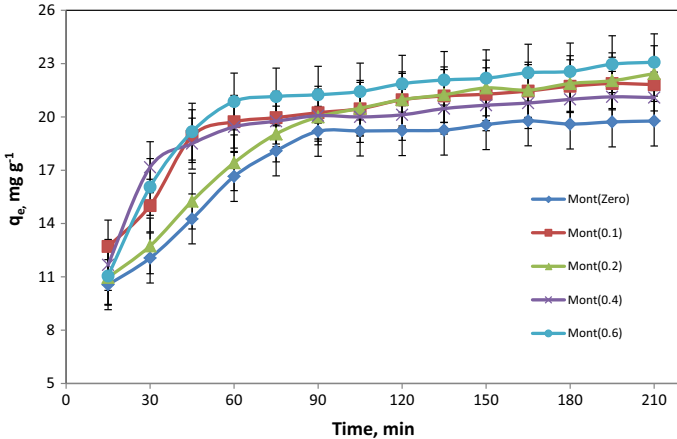
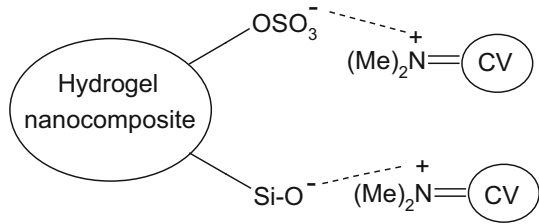


**Fig. 7** Effect of amount of NaMMT and contact time on CV adsorption

$\kappa$ C/PVA hydrogels, the dye adsorption capacity was decreased due to the decreased water absorbency of hydrogel [41]. In this study, the dye adsorption capacity was enhanced by the introduction of NaMMt, although the swelling capacity of nanocomposite was decreased.

Figure 7 also demonstrates the effect of contact time on CV adsorption capacity of the hydrogel nanocomposites. The adsorption capacity was increased versus agitation time up to 90 min and then, further increase in the agitation time had practically no remarkable effect on the  $q_e$ . It is obvious that increasing the adsorption time provides better opportunity for interaction between the adsorbent and the adsorbate. That is, the equilibrium is attained after 90 min, within the concentration range studied.

*Effect of salt solution on dye adsorption*

The presence of salt in dye solutions can affect the adsorption process. In this section of work, we studied the effect of different salts with the same concentration (0.15 M of NaCl, CaCl<sub>2</sub> and AlCl<sub>3</sub>) on CV adsorption. The effect of different salts on adsorption of CV on hydrogels is presented in Fig. 8. By introducing NaCl in dye solution, the adsorption capacity of hydrogels was slightly decreased. Most of dyes

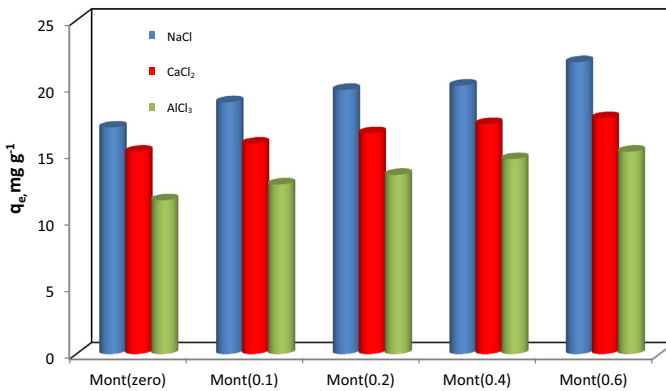


**Fig. 8** Effect of salt solution on CV adsorption

contain hydrophobic structure and the solubility of these dyes is reduced in the presence of salt, and mainly an enhancement in dye adsorption is observed [61]. This reduction in the solubility of dyes is originated from increasing in polarity of the solution. In contrast, in the adsorbents with ionic pendants, often a reduction in dye adsorption is obtained. The corresponding decrement in the dye adsorption capacity of nanocomposite hydrogels can be attributed to the neutralization or screening of anionic sulfate ( $-\text{OSO}_3^-$ ) groups on  $\kappa\text{C}$  by metal ions [61, 62]. This effect can result in a reduction in electrostatic interactions between cationic dye and anionic sulfate groups on adsorbent. In the dye solutions with  $\text{CaCl}_2$  and  $\text{AlCl}_3$  salts, the adsorption capacity of hydrogels for dye was significantly lower in comparison with  $\text{NaCl}$  solution. This behavior is due to the coordination of the  $\text{Ca}^{2+}$  and  $\text{Al}^{3+}$  ions with the anionic centers of hydrogels. These complexes can be led to a reduction in swelling of hydrogels and subsequently their diminished surface area. The reduction in surface of hydrogels can lead to a reduction in dye adsorption capacity.

#### *Effect of temperature on dye adsorption*

Thermodynamic parameters should be considered as important factors in the design of adsorption process. It is necessary to specify the change of thermodynamic parameters to estimate the feasibility and mechanism of adsorption process. So, thermodynamic parameters including standard Gibbs free energy ( $\Delta G$ ,  $\text{kJ mol}^{-1}$ ), enthalpy change ( $\Delta H$ ,  $\text{kJ mol}^{-1}$ ), and entropy change ( $\Delta S$ ,  $\text{J K}^{-1} \text{mol}^{-1}$ ) can be used for estimation of the feasibility adsorption process and are calculated according to the following equations [63]:

$$\ln K_D = \frac{\Delta S^\circ}{R} - \frac{\Delta H^\circ}{RT} \quad (3)$$



$$\Delta G^{\circ} = \Delta H^{\circ} - T\Delta S^{\circ} \quad (4)$$

where  $K_D$  is ratio of concentration of CV on adsorbent at equilibrium ( $q_e$ ) to the remaining concentration of the dye in solution at equilibrium ( $C_e$ ).  $\Delta H^{\circ}$  and  $\Delta S^{\circ}$  were obtained from slope and intercept of curve of plotting the  $\ln K_D$  versus  $1/T$ , respectively (Fig. 9). The calculated thermodynamic parameters for the adsorption of CV dye are presented in Table 2. The negative value of  $\Delta G^{\circ}$  at all the temperatures suggests that the adsorption of CV dye on the adsorbent is thermodynamically feasible and spontaneous in nature. Also, as the temperature increased from 298 to 318 K, the  $\Delta G^{\circ}$  values decreased, indicated high driving force and hence higher adsorption capacity at higher temperatures. The positive  $\Delta S^{\circ}$  value stipulates an increased randomness of the adsorbed dye molecules on nanocomposite surfaces. The negative values of  $\Delta H^{\circ}$  indicate that the adsorption is exothermic in nature. Therefore, due to electrostatically interactions between anionic sulfate groups of  $\kappa$ C and cationic CV molecules, the adsorption is spontaneous and exothermic.

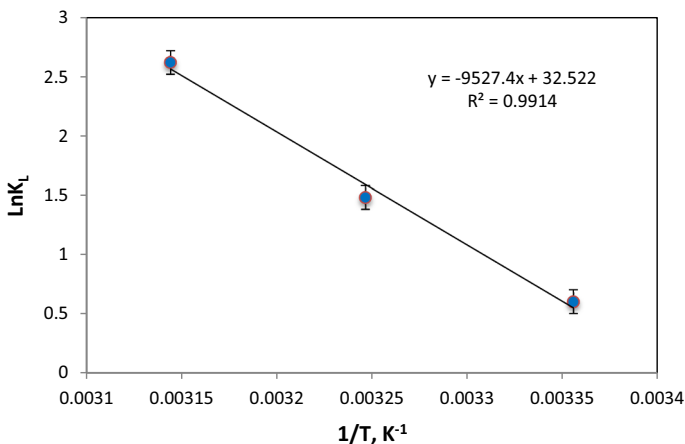
### Adsorption kinetics

The kinetic parameters are useful for the prediction of adsorption rate, which gives important information for the efficiency of adsorption. Therefore, to show the most suitable model for the experimental kinetic data, pseudo-first-order and pseudo-second-order kinetic models were used. The linear form of the pseudo-first-order rate equation is given as [57]:

$$\ln(q_e - q_t) = \ln q_{e1} - k_1 t \quad (5)$$

where  $q_e$  and  $q_t$  are the amounts of CV adsorbed ( $\text{mg g}^{-1}$ ) at equilibrium and at a predetermined time ( $t$ ), respectively.  $q_{e1}$  and  $k_1$  ( $\text{min}^{-1}$ ) show the theoretical equilibrium adsorption and rate constant of pseudo-first-order kinetic, respectively.

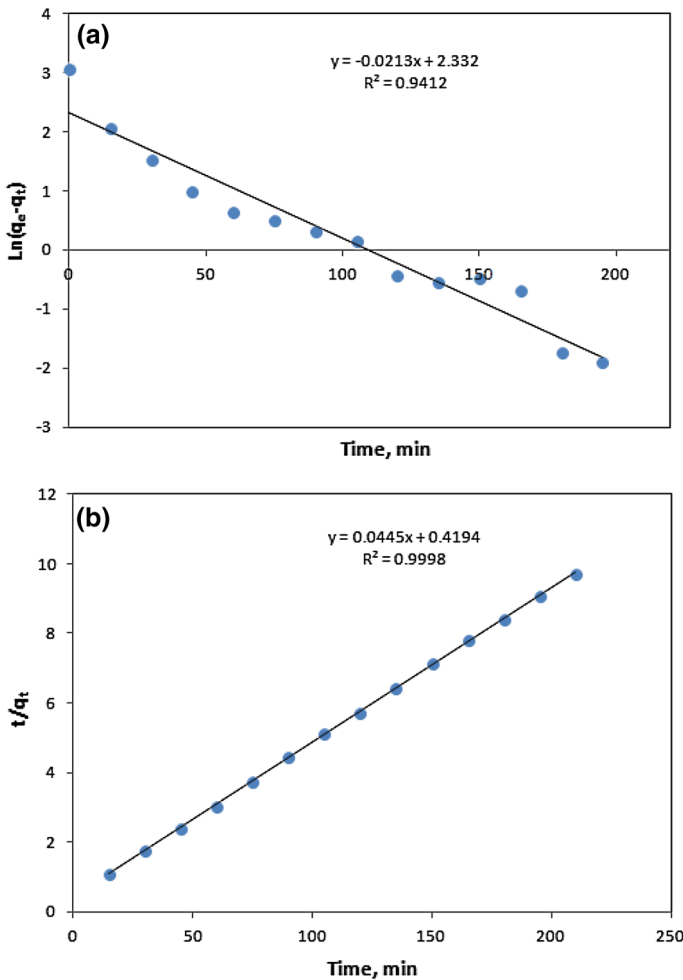
The linear form of the pseudo-second-order rate equation is expressed as [57]:



**Fig. 9** Plot of  $\ln K_L$  versus  $1/T$

**Table 2** Thermodynamic parameters for the adsorption of CV onto hydrogel nanocomposites containing 0.4 g content of NaMMT

$T$ (K)	Thermodynamic parameters			$R^2$
	$\Delta G^\circ$ (kJ mol $^{-1}$ )	$\Delta S^\circ$ (J K $^{-1}$ mol $^{-1}$ )	$\Delta H^\circ$ (kJ mol $^{-1}$ )	
298	−2			
308	−4	271	−79.258	0.9914
318	−6			

**Fig. 10** Plots of  $\ln(q_e - q_t)$  and  $t/q_t$  versus time in pseudo-first-order (a) and pseudo-second-order (b) equations for the hydrogel nanocomposite containing 0.1 g content of NaMMT

$$\frac{t}{q_t} = \frac{1}{k_2 q_{e2}^2} + \frac{t}{q_{e2}} \tag{6}$$

where  $k_2$  ( $\text{g mg}^{-1} \text{ min}^{-1}$ ) is the pseudo-second-order rate constant and  $q_{e2}$  is the theoretical adsorbed dye ( $\text{mg g}^{-1}$ ).

To obtain model calculations for pseudo-first-order and pseudo-second-order kinetics, we plotted  $\text{Ln}(q_e - q_t)$  against  $t$  and  $t/q_t$  against  $t$  (Fig. 10). The obtained kinetic parameters and correlation coefficients ( $R^2$ ) are summarized in Table 3. The fits of experimental kinetic data to the above-mentioned rate models were evaluated by  $R^2$ . The values of  $R^2$  for the pseudo-second-order model were  $\geq 0.998$  for all samples, and the adsorption capacities calculated ( $q_{e2}$ ) by this model were also closer to those determined by experiments ( $q_{e,exp}$ ). These results indicated better fit to pseudo-second-order than pseudo-first-order rate model to describe the adsorption process of CV on hydrogel nanocomposites. In fact, the pseudo-second-order model is based on the assumption that the rate-determining step may be a chemical sorption involving valence forces through sharing or the exchange of electrons between adsorbent and adsorbate.

### Adsorption isotherms

The adsorption isotherm expresses the correlation between the content of adsorbed dye on adsorbent and remained dye concentration at equilibrium time [46]. So, in this work, the experimental data from adsorption isotherms were fitted to non-linear Langmuir and Freundlich models to describe the adsorption process. Langmuir model describes monolayer adsorption of adsorbate on specific homogeneous sites within the adsorbent. This non-linear model is expressed by Eq. (7) [64]:

$$q_e = \frac{q_m K_L C_e}{1 + K_L C_e} \tag{7}$$

where  $C_e$  is the equilibrium dye concentration in the solution ( $\text{mg L}^{-1}$ ),  $K_L$  is the Langmuir adsorption constant related to the energy of adsorption ( $\text{L mg}^{-1}$ ), and  $q_m$  is the maximum adsorption capacity ( $\text{mg g}^{-1}$ ). Dimensionless constant adsorption parameter  $R_L$  as one of the essential characteristics of the Langmuir isotherm is expressed as follows [65]:

**Table 3** Constants of pseudo-first-order and pseudo-second-order rate models for CV adsorption onto hydrogel nanocomposites

	First-order kinetics			Second-order kinetics			$q_{e,exp}$
	$k_1 \times 10^{-3}$	$R^2$	$q_{e1}$	$k_2 \times 10^{-3}$	$R^2$	$q_{e2}$	
Mont (zero)	204.4	0.9689	19.57	53.2	0.9882	21.28	22.52
Mont (0.1)	17.7	0.8010	8.17	106.1	0.9998	22.47	22.89
Mont (0.2)	19.2	0.7689	13.02	44.2	0.9981	24.45	24.40
Mont (0.4)	16.0	0.6686	6.86	99.3	0.9995	22.12	22.52
Mont (0.6)	19.3	0.7048	7.55	95.8	0.9995	20.88	21.01

$$R_L = \frac{1}{1 + K_L C_o} \tag{8}$$

where  $K_L$  is the Langmuir constant ( $L\ mg^{-1}$ ) and  $C_o$  is the initial concentration of dye. In fact, the  $R_L$  value describes the type and shape of the isotherm [65] as summarized in Table 4.

Unlike the Langmuir model, in the Freundlich model the adsorption of adsorbate occurs on a heterogeneous surface by multilayer sorption. Non-linear Freundlich model is defined as follows [64]:

$$q_e = K_F C_e^{1/n} \tag{9}$$

where  $K_F$  is the equilibrium adsorption coefficient ( $mg\ g^{-1})(L\ mg^{-1})^{1/n}$  and  $1/n$  is the empirical constant. The  $n$  value depicts the favorability of adsorption process and  $K_F$  is related to the adsorption capacity of adsorbent.

The validity of models was estimated by regression coefficient [ $r^2$ , Eq. (10)] and Chi-square test [ $\chi^2$ , Eq. (11)] that obtained from the analysis of variance (ANOVA) in origin. A well fitting occurs when the  $r^2$  is close to unity and  $\chi^2$  be the lowest [66].

$$r^2 = \frac{(q_{i,meas} - \bar{q}_{i,cal})^2}{\sum_{i=1}^n (q_{i,meas} - \bar{q}_{i,cal})^2 + (q_{i,meas} - q_{i,cal})^2} \tag{10}$$

$$\chi^2 = \sum_{i=1}^n \frac{(q_{i,cal} - q_{i,meas})^2}{q_{i,meas}} \tag{11}$$

where  $q_{i,meas}$  and  $q_{i,cal}$  are the experimental and calculated amount of dye adsorption, respectively. The  $\bar{q}_{cal}$  value indicates the average of  $q$  calculated theoretically.

**Table 4**  $R_L$  values and isotherms

$R_L$ value	Type of isotherm
$R_L > 1$	Unfavorable
$R_L = 1$	Linear
$0 < R_L < 1$	Favorable
$R_L = 0$	Irreversible

**Table 5** Constants parameters of isotherm models for adsorption of CV on hydrogels

	Freundlich model				Langmuir model					$q_{m,exp}$
	$n$	$K_F$	$\chi^2$	$r^2$	$q_m$	$K_L$	$\chi^2$	$r^2$	$R_L$	
Mont (zero)	4.16	71.5	46.2	0.79	134	0.067	0.73	0.92	0.37	125
Mont (0.1)	2.94	40.5	1.09	0.73	145	0.127	0.0025	0.96	0.24	145
Mont (0.2)	2.76	36.7	0.02	0.82	150	0.016	$7 \times 10^{-5}$	0.95	0.71	151
Mont (0.4)	1.55	9.16	1.66	0.98	140	0.120	0.185	0.99	0.25	135
Mont (0.6)	8.33	56.2	4.30	0.80	140	0.020	0.17	0.99	0.66	145

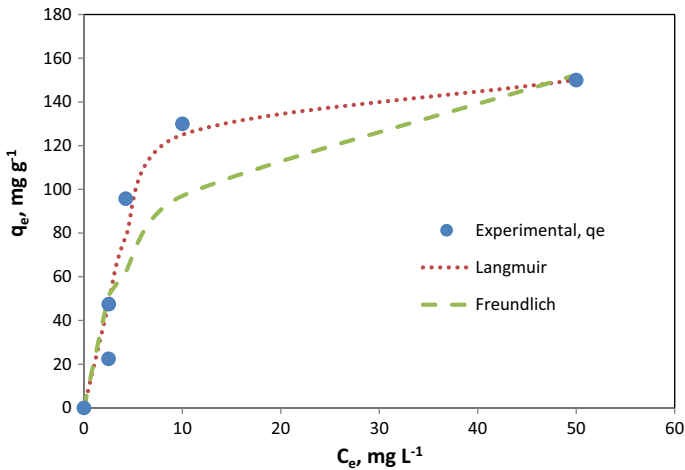


**Fig. 11** Comparison between the experimental and modeled isotherms plots for adsorption of CV dye onto the hydrogel nanocomposite containing 0.2 g content of NaMMT

The adsorption constant parameters,  $r^2$  and  $\chi^2$  obtained after fitting the adsorption isotherm data to Langmuir and Freundlich models are summarized in Table 5. Figure 11 displays curves comparing the modeled adsorption isotherms with practical data. According to Fig. 11, it was observed that the adsorption of dye on hydrogels followed well the Langmuir model than that of the Freundlich model. Moreover, according to the data from Table 5, the values of regression coefficient  $r^2$  (close to unity,  $r^2 > 0.98$ ) and Chi-square test  $\chi^2$  (low value) confirmed the well fitting of experimental data to Langmuir model. In addition, the maximum adsorption capacity of hydrogels obtained from Langmuir model was relatively in agreement with experimental data. This fitting revealed that a monolayer adsorption of dye takes place on hydrogel adsorbents. The values of  $R_L$  for hydrogels were also calculated from Langmuir model and were found to be between 0 and 1 indicating favorable adsorption system (see also Table 4).

Finally, the maximum adsorption capacity of the present work is compared with other dye adsorbents reported in the literatures as given in Table 6. According to these data, the adsorption capacity of the hydrogel nanocomposites prepared in this study was comparable with that of other adsorbents.

## Conclusion

In the present research, a new hydrogel nanocomposite composed of *kappa*-carrageenan and poly(vinyl alcohol) was synthesized by freezing–thawing method in the presence of sodium montmorillonite. Specific interactions of NaMMT with functional groups of  $\kappa$ C and PVA through hydrogen bonding were estimated by FTIR. Also, XRD and TEM showed a layered morphology due to the penetration of

**Table 6** Comparison of sorption capacity of CV on various adsorbents

	Adsorbent	Adsorption capacity (mg g <sup>-1</sup> )	References
	Raw kaolin	26	[67]
	Bagasse fly ash	79	[68]
	Magnetic $\kappa$ -Carb <sup>a</sup>	85	[43]
	CarAlg/MMT <sup>b</sup>	89	[46]
	Activated carbon	65	[69]
<sup>a</sup> Magnetic <i>kappa</i> -carrageenan beads	Sewage sludge	263	[70]
<sup>b</sup> Carrageenan-alginate/montmorillonite nanocomposite hydrogels	Raw bentonite	130	[71]
	Modified bentonite	457	[71]
<sup>c</sup> Chitosan- <i>g</i> -(4-hydroxybenzoic acid)	Chitosan-BA <sup>c</sup>	18	[72]
	PVBC beads <sup>d</sup>	150	[73]
<sup>d</sup> Poly(vinyl benzyl chloride) beads	Ball clay	169	[74]
	$\kappa$ C-PVA/NaMMT	151	Present work

polymer chains into NaMMT silicate layers. According to XRD and TEM results, the nanoclay showed intercalated and exfoliated structure.

The modified hydrogel nanocomposite was then used for removal of crystal violet from aqueous solution. The adsorption capacity of nanocomposites was found to vary with content of NaMMT, pH, salt solution, and contact time as well as temperature of solution. Thermodynamic parameters also indicated that the adsorption was spontaneous and endothermic in nature.

Moreover, the fitting of experimental kinetic data to rate models showed that the pseudo-second-order model was the best fitted than the pseudo-first-order model in adsorption of CV onto nanocomposites. Besides, the data indicated that the CV adsorption onto the hydrogel nanocomposites obeys the Langmuir isotherm model. According to this model, maximum dye adsorption capacity was achieved 151 mg g<sup>-1</sup>.

Overall, the obtained results suggested that the hydrogel nanocomposites synthesized in this work could be used as an effective adsorbent for adsorption of CV in the field of wastewater treatment.

## References

- White JL, Bumm SH (2011) Polymer blend compounding and processing. In: Isayev AI, Palsule S (eds) Encyclopedia of polymer blends. Wiley-VCH, Weinheim, pp 1–26
- Xie Y, Wang A (2009) Study on superabsorbent composites XIX. Synthesis, characterization and performance of chitosan-*g*-poly (acrylic acid)/vermiculite superabsorbent composites. J Polym Res 16:143–150
- Bagheri Marandi G, Mahdavinia GR, Ghafary S (2011) Collagen-*g*-poly (sodium acrylate-*co*-acrylamide)/sodium montmorillonite superabsorbent nanocomposites: synthesis and swelling behavior. J Polym Res 18:1487–1499
- Hassine K, Durmus A, Kasgoz A (2008) Enhanced swelling and adsorption properties of AAm-AMPSNa/clay hydrogel nanocomposites for heavy metal ion removal. Polym Adv Technol 19:213–220

5. Sperling LH (2012) Interpenetrating polymer networks and related materials. Springer, New York
6. Demirel G, Ozcetin G, Sahin F, Tunturk H, Aksoy S, Hasirci N (2006) Semi-interpenetrating polymer networks (IPNs) for entrapment of glucose isomerase. *React Funct Polym* 66:389–394
7. Kirk RE, Othmer DF (1992). Encyclopedia of chemical technology. In: Kroschwitz JI, Howe-Grant M (eds) vol 4, 4th edn. Wiley, New York, p 942
8. Takemasa M, Chiba A, Date M (2002) Counter ion dynamics of  $\kappa$ - and  $\iota$ -carrageenan aqueous solutions investigated by the dielectric properties. *Macromolecules* 35(14):5595–5600
9. Antonov YA, Goncalves MP (1999) Phase separation in aqueous gelatin-carrageenan systems. *Food Hydrocoll* 13:517–524
10. Araujo JV, Davidenko N, Danner M, Cameron RE, Best SM (2014) Novel porous scaffolds of pH responsive chitosan/carrageenan-based polyelectrolyte complexes for tissue engineering. *J Biomed Mater Res A* 102:4415–4426
11. Park JS, Park JW, Ruckenstein E (2001) Thermal and dynamic mechanical analysis of PVA/MC blend hydrogels. *Polymer* 42:4271–4280
12. Peppas NA, Stauffer SR (1991) Reinforced uncrosslinked poly (vinyl alcohol) gels produced by cyclic freezing-thawing processes: a short review. *J Control Release* 16:305–310
13. Yokoyama F, Masada I, Shimamura K, Ikawa T, Monobe K (1986) Morphology and structure of highly elastic poly (vinyl alcohol) hydrogel prepared by repeated freezing-and melting. *Colloid Polym Sci* 26:595–601
14. Kim JO, Park JK, Kim JH, Jin SG, Yonga CS, Li DX, Choi JY, Woo JS, Yoo BK, Lyoo WS, Kim JA, Choi HG (2008) Development of poly(vinyl alcohol-sodium alginate gel-matrix-based wound dressing system containing nitrofurazone. *Int J Pharm* 359:79–86
15. Buchholz FL, Graham AT (1997) Modern superabsorbent polymer technology. Wiley, New York
16. Singh B, Pal L (2008) Development of sterculia gum based wound dressings for use in drug delivery. *Eur Polym J* 44:3222–3230
17. Sorbara L, Jones L, Williams LD (2009) Contact lens induced papillary conjunctivitis with silicone hydrogel lenses. *Contact Lens Anter Eye* 32:93–96
18. Mao L, Hu Y, Piao Y, Chen X, Xian W, Piao D (2005) Structure and character of artificial muscle model constructed from fibrous hydrogel. *Curr Appl Phys* 5:426–428
19. Lee CT, Kung PH, Lee YD (2005) Preparation of poly (vinyl alcohol)-chondroitin sulfate hydrogel as matrices in tissue engineering. *Carbohydr Polym* 61:348–354
20. Wu J, Wei W, Lian YW, Su ZG, Ma GH (2007) A thermosensitive hydrogel based on quaternized chitosan and poly(ethylene glycol) for nasal drug delivery system. *Biomaterials* 28:2220–2232
21. Lin Y, Chen Q, Luo H (2007) Preparation and characterization of *N*-(2-carboxybenzyl) chitosan as a potential pH-sensitive hydrogel for drug delivery. *Carbohydr Res* 342:87–95
22. Crini G (2005) Recent developments in polysaccharide-based materials used as adsorbents in wastewater treatment. *Prog Polym Sci* 30:38–70
23. Kim SS, Lee YM, Cho CS (1995) Semi-interpenetrating polymer networks composed of  $\beta$ -chitin and poly(ethylene glycol) macromer. *J Polym Sci A Polym Chem*. 33:2285–2287
24. Farshi Azhar F, Olad A, Mirmohseni A (2014) Development of novel hybrid nanocomposites based on natural biodegradable polymer–montmorillonite/polyaniline: preparation and characterization. *Polym Bull* 71:1591–1610
25. Yuanqing X, Zhiqin P (2006) A new polymer/clay nano-composite hydrogel with improved response rate and tensile mechanical properties. *Eur Polym J* 42:2125–2132
26. Mahdavinia GR, Asgari A (2013) Synthesis of *kappa*-carrageenan-*g*-poly(acrylamide)/sepiolite nanocomposite hydrogels and adsorption of cationic dye. *Polym Bull* 70:2451–2470
27. Zhang Q, Li X, Zhao Y, Chen L (2009) Preparation and performance of nanocomposite hydrogels based on different clay. *Appl Clay Sci* 46:346–350
28. Yi J, Ma Y, Zhang L (2008) Synthesis and decoloring properties of sodium humate/poly (*N*-isopropylacrylamide) hydrogels. *Bioresour Technol* 99:5362–5367
29. Kaplan M, Kasgoz H (2011) Hydrogels nanocomposite sorbents for removal of basic dyes. *Polym Bull* 67:1153–1168
30. Xiang YQ, Peng ZQ, Chen DJ (2006) A new polymer/clay nano-composite hydrogel with improved response rate and tensile mechanical properties. *Eur Polym J* 42:2125–2132
31. Wu JH, Wei YL, Lin JM, Lin SB (2003) Study on starch-graft-acrylamide/mineral powder super-absorbent composite. *Polymer* 44:6513–6520
32. Sanghi R, Bhattacharya B (2002) Review on decolorization of aqueous dye solutions by low cost adsorbents. *Color Technol* 118:256–269

33. Dotto GL, Pinto LAA (2011) Adsorption of food dyes onto chitosan: optimization process and kinetic. *Carbohydr Polym* 84:231–238
34. Zhu HY, Jiang R, Xiao L, Li W (2010) A novel magnetically separable c-Fe<sub>2</sub>O<sub>3</sub>/crosslinked chitosan adsorbent: preparation, characterization and adsorption application for removal of hazardous azo dye. *J Hazard Mater* 179:251–257
35. Luo X, Zhang L (2009) High effective adsorption of organic dyes on magnetic cellulose beads entrapping activate carbon. *J Hazard Mater* 171:340–347
36. Sui K, Li Y, Liu R, Zhang Y, Zhao X, Liang H, Xia Y (2012) Biocomposite fiber of calcium alginate/multi-walled carbon nanotubes with enhanced adsorption properties for ionic dyes. *Carbohydr Polym* 90:399–406
37. Wan Ngah WS, Teong LC, Hanafiah MAKM (2011) Adsorption of dyes and heavy metal ions by chitosan composites: a review. *Carbohydr Polym* 83:1446–1456
38. Sirousazar M, Kokabi M, Hassan ZM (2012) Swelling behavior and structural characteristics of poly(vinyl alcohol)/montmorillonite nanocomposite hydrogels. *J Appl Polym Sci* 123:50–58
39. Sirousazar M, Kokabi M, Hassan ZM, Bahramian AR (2012) Poly(vinyl alcohol)/Na-montmorillonite nanocomposite hydrogels prepared by freezing-thawing method: structural, mechanical, thermal, and swelling properties. *J Macromol Sci B Phys* 51:71335–71350
40. Ip KH, Stuart BH, Ray TA (2011) Characterization of poly(vinyl alcohol)–montmorillonite composites with higher clay contents. *Polym Test* 30:732–736
41. Mahdavinia GR, Masoudi A, Baghban A (2014) Study on adsorption of cationic dye on magnetic *kappa*-carrageenan/PVA nanocomposite hydrogels. *J Environ Chem Eng* 2:1578–1587
42. Muhamad II, Fen LS, Hui NH, Mustapha NA (2011) Genipin-cross-linked *kappa*-carrageenan/carboxymethyl cellulose beads and effects on beta-carotene release. *Carbohydr Polym* 83:1207–1212
43. Mahdavinia GR, Irvani S, Zoroufi S, Hosseinzadeh H (2014) Magnetic and K<sup>+</sup>-cross-linked *kappa*-carrageenan nanocomposite beads and adsorption of crystal violet. *Iran Polym J* 23:335–344
44. Mahdavinia GR, Massoudi A, Baghban A, Massoumi B (2012) Novel carrageenan-based hydrogel nanocomposites containing laponite RD and their application to remove cationic dye. *Iran Polym J* 21:609–619
45. Mahdavinia GR, Bagheri-Marandi G, Kiani G, Pourjavadi A (2010) Semi-IPN carrageenan-based nanocomposite hydrogels: synthesis and swelling behavior. *J Appl Polym Sci* 118:2989–2997
46. Mahdavinia GR, Aghaie H, Sheykhloie H, Vardini MT, Etemadi H (2013) Synthesis of CarAlg/MMt nanocomposite hydrogels and adsorption of cationic crystal violet. *Carbohydr Polym* 98:358–365
47. Deng S, Xu H, Jiang X, Yin J (2013) Poly(vinyl alcohol) (PVA)-enhanced hybrid hydrogels of hyperbranched poly(ether amine) (hPEA) for selective adsorption and separation of dyes. *Macromolecules* 46:2399–2406
48. Hassan CM, Peppas NA (2000) Structure and applications of poly(vinyl alcohol) hydrogels produced by conventional crosslinking or by freezing/thawing methods. *Adv Polym Sci* 153:37–65
49. Holloway JL, Lowman AM, Palmese GR (2013) The role of crystallization and phase separation in the formation of physically cross-linked PVA hydrogels. *Soft Matter* 9:826–833
50. Hernandez R, Lopez D, Mijangos C, Guenet JM (2002) A reappraisal of the ‘thermoreversible’ gelation of aqueous poly(vinyl alcohol) solutions through freezing-thawing cycles. *Polymer* 43:5661–5663
51. Gonzalez JS, Alvarez VA (2011) The effect of the annealing on the poly(vinyl alcohol) obtained by freezing–thawing. *Thermochim Acta* 521:184–190
52. Mallapragada SK, Peppas NA (1996) Dissolution mechanism of semicrystalline poly(vinylalcohol) in water. *J Polym Sci B Polym Phys* 34:1339–1346
53. Morris R, Rees DA, Robinson G (1980) Cation-specific aggregation of carrageenan helices: domain model of polymer gel structure. *J Mol Biol* 138:349–362
54. Pass G, Phillips OG, Wedlock DJ (1977) Interaction of univalent and divalent cations with carrageenans in aqueous solution. *Macromolecules* 10:197–201
55. Bongaerts K, Reynaers H, Zanetti F, Paoletti S (1999) Equilibrium and nonequilibrium association processes of  $\kappa$ -carrageenan in aqueous salt solutions. *Macromolecules* 32:683–689
56. Darvishi Z, Kabiri K, Zohuriaan-Mehr MJ, Morsali A (2011) Nanocomposite super-swelling hydrogels with nanorod bentonite. *J Appl Polym Sci* 120:3453–3459
57. Chatterjee S, Chatterjee T, Lim SR, Woo SH (2011) Effect of the addition mode of carbon nanotubes for the production of chitosan hydrogel core-shell beads on adsorption of Congo red from aqueous solution. *Bioresour Technol* 102:4402–4409
58. Bredy JE, Holum JR (1993) *Chemistry*. Wiley, New York



59. Gu YS, Decker EA, McClements DJ (2005) Influence of pH and carrageenan type on properties of beta-lactoglobulin stabilized oil-in-water emulsions. *Food Hydrocoll* 19:83–89
60. Monvisade P, Siriphannon P (2009) Chitosan intercalated montmorillonite: preparation, characterization and cationic dye adsorption. *Appl Clay Sci* 42:427–431
61. Hu Y, Guo T, Ye X, Li Q, Guo M, Liu H, Wu Z (2013) Dye adsorption by resins: effect of ionic strength on hydrophobic and electrostatic interactions. *Chem Eng J* 228:392–397
62. Li Q, Yue Q, Sun H, Su Y, Gao B (2010) A comparative study on the properties, mechanisms and process designs for the adsorption of non-ionic or anionic dyes onto cationic-polymer/bentonite. *J Environ Manag* 91:1601–1611
63. Ozcan A, Oncu EM, Ozcan S (2006) Adsorption of acid blue 193 from aqueous solutions onto DEDMA-sepiolite. *J Hazard Mater B* 129:244–252
64. Piccin JS, Gomes CS, Feris LA, Gutterres M (2012) Kinetics and isotherms of leather dye adsorption by tannery solid waste. *Chem Eng J* 183:30–38
65. Hameed BH, Ahmad AA, Aziz N (2007) Isotherms, kinetics and thermodynamics of acid dye adsorption on activated palm ash. *Chem Eng J* 133:195–203
66. Foo KY, Hameed BH (2010) Insights into the modeling of adsorption isotherm systems. *J Chem Eng* 156:2–10
67. Nandi BK, Goswami A, Das AK, Mondal B, Purkait MK (2008) Kinetic and equilibrium studies on the adsorption of crystal violet dye using kaolin as an adsorbent. *Sep Sci Technol* 43:1382–1403
68. Mall ID, Srivastava VC, Agarwal NK (2006) Removal of Orange-G and Methyl Violet dyes by adsorption onto bagasse fly ash—kinetic study and equilibrium isotherm analyses. *Dyes Pigm* 69:210–223
69. El-Guendi M (1991) Adsorption of basic dye using activated carbon prepared from oil palm. *Adsorpt Sci Technol* 8:217–225
70. Otero M, Rozada F, Calvo LF, García AI, Morán A (2003) Elimination of organic water pollutants using adsorbents obtained from sewage sludge. *Dyes Pigm* 57:55–65
71. Eren E (2009) Removal of basic dye by modified Unye bentonite, Turkey. *J Hazard Mater* 162:1335–1363
72. Chao A, Shyu S, Lin Y, Mi F (2004) Enzymatic grafting of carboxyl groups on to chitosan to confer on chitosan the property of a cationic dye adsorbent. *Bioresour Technol* 91:157–162
73. Kaner D, Sarac A, Senkal BF (2010) Removal of dyes from water using crosslinked aminomethane sulfonic acid based resin. *Environ Geochem Health* 32:321–325
74. Monash P, Niwas R, Pugazhenthii G (2011) Utilization of ball clay adsorbents for the removal of crystal violet dye from aqueous solution. *Clean Technol Environ Policy* 13:141–151